Proceedings of The Joint Canadian Society for Mechanical Engineering and CFD Society of Canada International Congress 2019
CSME-CFDSC Congress 2019
June 2-5, 2019, London, On, Canada

WRF SIMULATIONS OF URBAN CLIMATE: DO WE NEED LOW OR HIGH TOPOGRAPHIC RESOLUTION?

Md. Rafsan Nahian[1], Amir Nazem[2], Mohsen Moradi[3], Shohel Mahmud[4], William D. Lubitz[5], Amir A. Aliabadi[*]
School of Engineering
University of Guelph
Guelph, Canada
[1]mnahian@uoguelph.ca, [2]anazem@uoguelph.ca, [3]moradim@uoguelph.ca, [4]smahmud@uoguelph.ca, [5]wlubitz@uoguelph.ca,
[*]Corresponding Author: aliabadi@uoguelph.ca

Abstract— The performance of the Weather Research and Forecasting (WRF) model is evaluated with low and high topographic resolutions to observe the urban climate both in the surface level and higher altitudes. Overall, the model has presented a better performance in predicting the heat related properties compared to the momentum related properties. It has been observed that high wind bias is one of the main limitations of the model and the bias is higher at surface level compared to higher altitudes. High topographic resolution WRF simulations show better agreements with experimental observations in terms of predicting horizontal wind velocity while low topographic resolution WRF simulations deliver better results for reanalysis of the vertical wind velocity. Low topographic resolution WRF simulations predict relative humidity closer to experimental measurements while high topographic resolution WRF simulations predict surface level potential temperature more accurately. Overall, it is found that WRF under predicts the vertical wind velocity, potential temperature, and relative humidity while it over predicts the horizontal wind velocity both in surface level and higher elevations.

Keywords-component; WRF; mesoscale model; urban climate; GEOTPO 30 s; SRTM 1 s

I. INTRODUCTION

The Weather Research and Forecasting (WRF) model is a numerical weather prediction (NWP) mesoscale model designed for both research and operational atmospheric applications. It is suitable for an extensive span of applications across scales ranging from large eddy to global simulations. Such applications include real time NWP, data assimilation development and studies, parameterized physics research, regional climate simulations, air quality modeling, atmosphere-ocean-coupled simulations, and idealized simulations. In WRF, it is possible to combine and match the dynamical cores and physics packages of various models to optimize performance and this feature is particularly advantageous for intermodal comparisons and sensitivity studies [1].

The Weather Research and Forecasting (WRF) model has presented a high wind speed bias over land since the early versions of the model [2]. It has been identified that the bias still exists in the latest versions which represents a limitation for the high demand of accurate wind estimations by different sectors [3]. Since current atmospheric models present an extensive spectrum of configuration options and parameters, selecting the optimum configuration among these alternatives has its own inherent challenges [4].

Researchers have emphasized the importance of the sensitivity of a model to change in its configuration settings. Various model configurations and parameter settings along with different initialization fields have been evaluated in this study [5]. WRF can be used for short term forecasting, reanalysis, assimilating in situ LIDAR observations and selecting the appropriate planetary boundary layer (PBL) scheme for a complex terrain [6]. It is shown that error minimization in the WRF simulation can be achieved by testing and choosing a suitable numerical and physical configuration for the region of interest. Increasing the horizontal and vertical grid resolution may lead to better reproduction of fine scale meteorological processes but this may not necessarily be true due to uncertainties in the overall performance of the various physical parameterizations and their responses to grid resolution [7].

Several physical parameterization schemes are available for microphysics, radiation and clouds, planetary boundary layer (PBL) schemes, surface layer (SL), and the land surface model (LSM). Such schemes have nonlinear interactions with each other and with the dynamical core of the model. Therefore, it becomes challenging to optimize the model due to these complex relationships [1]. Therefore, the effect of such non-linearities on the simulation results cannot be predicted without performing the simulation. Also, such nonlinearities may cause model divergence. As a result, the effects must be investigated by parametric simulations. Model errors consist of the dependence on different numerical solvers, domain sizes, site location, initialization, boundary conditions, terrain and vegetation characteristics, and grid resolution both in horizontal and vertical directions [8]. Another important factor is the topography which has a great influence on the climate of a region. The substantial orographic features greatly influence the local and global weather and climate by changing the dynamics of the atmospheric circulation and interactions between the atmosphere and the land surface [9].

In most of the existing literature, the low topographic resolution (Global 30 Arc-Second) data-set has been applied to run WRF simulations and the results are compared with surface level observations. It is still a challenge for researchers to initialize high topographic resolution datasets for WRF simulations as well as observing the atmospheric properties in higher altitudes due to the complexity and unavailability of expensive weather sensing instruments. Hence, the main objectives of this paper are to observe the urban atmospheric boundary layer both near surface level and higher elevations to test the capability of WRF model using low and high topographic resolutions, and to observe the diurnal variations of different momentum and heat related properties. Subsequently, the numerical outcomes are compared with experimental observations of different meteorological instruments to compute the bias and error of the WRF model.

II. METHODOLOGY

A. Domain configurations

A particular distribution of WRF titled the Unified Environmental Modelling System (UEMS) version 18.8.1 has been tested with various grid configurations including the way of nesting, grid resolution, time invariant data resolution and geographical shifts in the domain center. The minimum grid distance of the nested domains should be at least four grid cells from parent boundary [10]. For computational stability, the magnitude of time steps (in seconds) are prescribed as the maximum 6 times the magnitude of the coarsest grid distance. This rule is associated with the coarsest grid and the time step is divided by 3 in each nest to maintain a ratio of 1/3 [1].

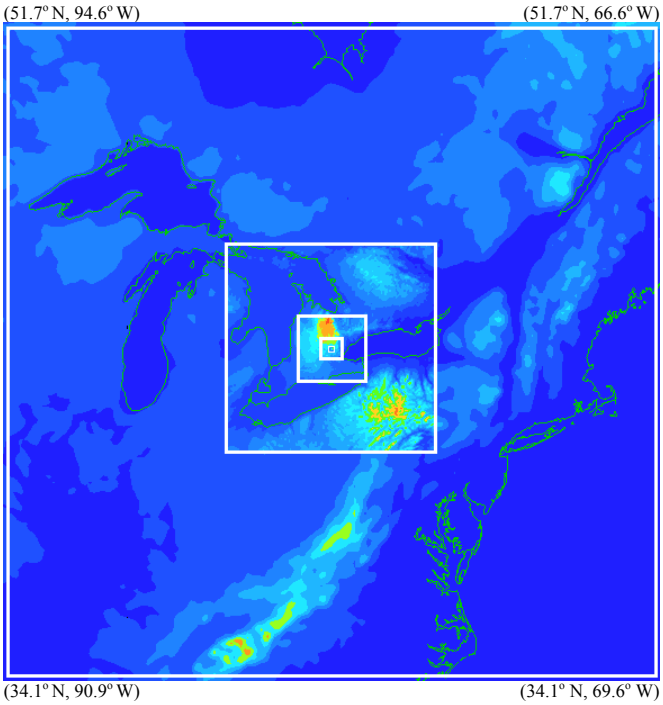

Figure 1. Size of the nested domains with Latitude and Longitude centered at Guelph, Ontario, Canada

Fig. 1 and Table I illustrate the size and configuration of the domains, respectively, where domain 1 is the largest domain and domain 5 is the smallest one. 45 vertical levels are used as opposed to more levels to gain computational speed.

TABLE I. CONFIGURATIONS OF THE NESTED DOMAINS

Parameter	Domain number				
	Domain 1	***Domain 2***	***Domain 3***	***Domain 4***	***Domain 5***
Domain size (km × km)	2000	633	198	61.4	18.4
Grid size (km)	10	3.33	1.11	0.37	0.12
Number of grid elements	200	190	178	166	154
Top of the domain (km)	25	25	25	25	25
Vertical levels	45	45	45	45	45
Output frequency (minute)	60	60	60	60	60
GTOPO 30s topographical resolution (m)	900	900	900	900	900
SRTM 1s topographical resolution (m)	900	900	900	30	30

B. Intialization

The WRF simulations are run for three different days on August 03, 04, and 13 in 2018, for 36 hours including a spin up time of 12 hours. The Global Forecasting System (GFS) data-set has been used in the simulation that provides initial and time varying boundary conditions to WRF every three hours. WRF provides the option for obtaining time varying meteorological initialization fields from different sources. These sources of initialization fields provide data at different topographic resolutions and these predicted atmospheric properties are the critical aspect of this study.

The Global 30 Arc-Second (GTOPO 30s) and the Shuttle Radar Topography Mission 1 Arc-Second (SRTM 1s) datasets are used to modify the resolution of topography in domain 4 and domain 5. GTOPO 30s is a global dataset covering the full extent of latitude from 90 degrees south to 90 degrees north, and the full extent of longitude from 180 degrees west to 180 degrees east. As a low topographic initialization, the GTOPO 30s has geographic resolution around 900 m × 900 m. On the other hand, the Shuttle Radar Topography Mission (SRTM) is an international research effort that obtained digital elevation models on a near-global scale to generate the most complete high-resolution digital topographic database of the Earth. The SRTM 1s data-set has topographic resolution of about 30 m × 30 m, which is 30 times higher than the GTOPO 30s dataset [11]. Moreover, time invariant data including land water masks, land use, land cover classification and albedo have been obtained from the NCAR and MODIS database at all available resolutions. The surface height of domain 5 from sea level for both GTOPO 30 s and SRTM 1s datasets are shown in Fig. 2 and Fig. 3 respectively.

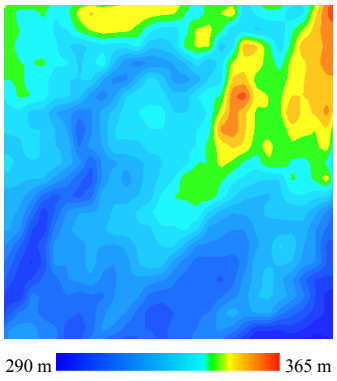

Figure 2. Surface height from sea level (GEOTOPO 30s)

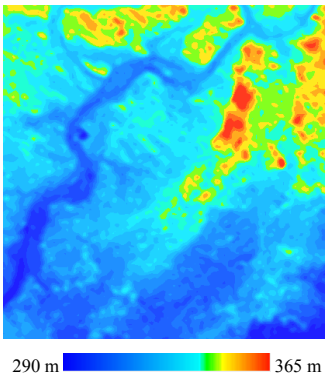

Figure 3. Surface height from sea level (SRTM 1s)

C. *Physical options*

The planetary boundary layer (PBL) scheme implemented in the model plays a decisive role on the accuracy of reanalyzed state and flow within the PBL because the wind varies according to the stability and baroclinic instability of the PBL. Some researchers have studied performing a sensitivity test of the WRF model and found that the Yonsei University scheme (YSU) shows improvement over the other PBL schemes of WRF [7, 12]. Hence, YSU scheme is applied in the simulation which uses identical profile functions for momentum and heat assuming turbulent Prandtl number as a constant.

D. *Validation*

The results of WRF model should be verified because of the uncertainty in model implementation for any specific location. Hence, experimental datasets from a Mini SODAR 4000 series by Atmospheric Systems Corporation located in the Turfgrass area at Guelph are used to validate the WRF simulations in higher elevation wind for every 4 hours while Guelph Turfgrass weather station's hourly dataset is used for surface level. The Guelph Turfgrass Institute station is identified with World Meteorological Organization (WMO) identification number 71833. This data is accessible with an hourly time resolution. Temperature data is collected at 2 m while wind data is collected at 10 m above the ground [13].

A quantitative comparison between the experimental observations and WRF model is performed by determining the Bias, Fractional Bias (FB) and the Normalized Mean Square Error (NMSE) [14] defined by

$$\text{BIAS} = \frac{\sum_{i=1}^{n} O_i - \sum_{i=1}^{n} M_i}{n}, \tag{1}$$

$$\text{FB} = \frac{\sum_{i=1}^{n} O_i - \sum_{i=1}^{n} M_i}{0.5\,(\sum_{i=1}^{n} O_i + \sum_{i=1}^{n} M_i)}, \tag{2}$$

$$\text{NMSE} = \frac{\sum_{i=1}^{n} (O_i - M_i)^2}{(\sum_{i=1}^{n} O_i)(\sum_{i=1}^{n} M_i)}. \tag{3}$$

Here, O and M represent the experimental observation and WRF model, respectively, while n represents the number of sample. Furthermore, for wind direction, the bias is calculated differently because wind direction is a circular variable. For each model (M) and observation (O) comparison, the bias is calculated using

$$\text{BIAS} = (|O\text{-}M|)\ \%\ 180. \tag{4}$$

Here all angles are in degrees and the remainder of a positive difference is taken by dividing this difference with 180 degrees. This ensures that the difference is always between 0 and 180 degrees. Of course, for multiple comparisons an average or median can be taken for this bias.

III. Results and Discussion

The comparison between WRF simulations in domain 5 and the experimental observations on August 3, 4 and 13, 2018 is evaluated in this discussion. In each time interval, the median value of every property is considered to perform statistical analysis because the mean value may not be a fair representation of the data due to the mean value being easily influenced by the outlines in the data.

A. *Horizontal wind velocity*

Horizontal wind speed is a fundamental atmospheric field property caused by air moving from high to low pressure. The dispersion process of pollutants in any region is highly affected by wind speed where diffusion takes place in the direction of plume transport [15]. Figs. 4-6 show the fractional bias of horizontal wind speed at 10 m (near surface level), 70 m (Mini SODAR) and 170 m (Mini SODAR) respectively. These altitudes are pressure heights[1]. In these figures the error bars represent the Normalized Mean Square Error (NMSE).

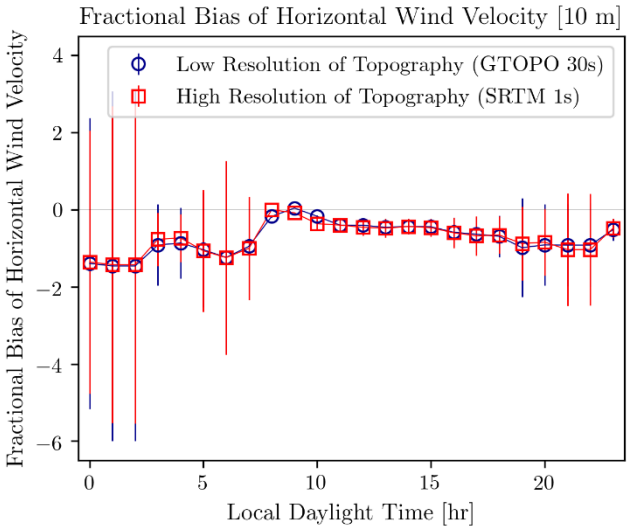

Figure 4. Fractional bias of horizontal wind velocity at 10 m

[1] www.weather.gov/epz/wxcalc_pressurealtitude

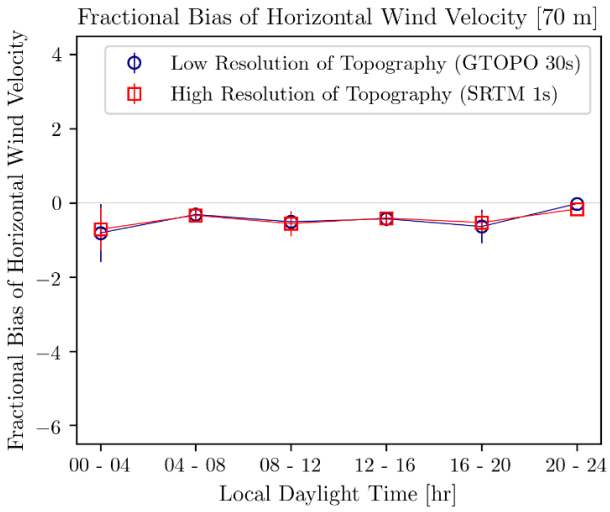

Figure 5. Fractional bias of horizontal wind velocity at 70 m

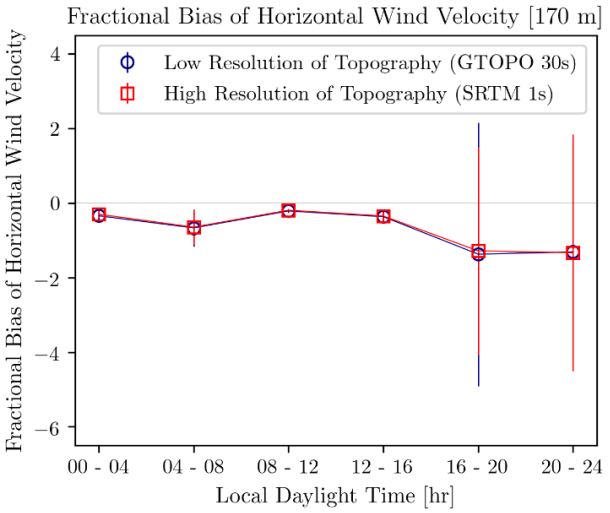

Figure 6. Fractional bias of horizontal wind velocity at 170 m

It has been observed that in convective hours when the atmosphere is thermally unstable, WRF shows less fractional bias and error than the thermally stable conditions at late night and early morning. There are no significant differences between low and high topographic resolution WRF simulations although at 10 m elevation high topographic resolution WRF simulations sometimes show marginally better agreement than the low topographic resolution WRF simulations. Low altitude wind speeds at surface level are influenced by surface roughness and atmospheric stability. Low topographic resolution WRF simulations do not account for realistic surface roughness in the topography and therefore exhibit unwanted bias in wind speed compared to high topographic resolution WRF simulations.

B. Vertical wind speed

Vertical velocity is a key factor for cloud development, precipitation, and development of weather systems. Figs. 7-8 show the fractional bias of vertical wind speed at 70 m (Mini SODAR) and 170 m (Mini SODAR), respectively. It is also noted that the 10 m observation does not include vertical wind speed. In these figures the error bars represent the Normalized Mean Square Error (NMSE).

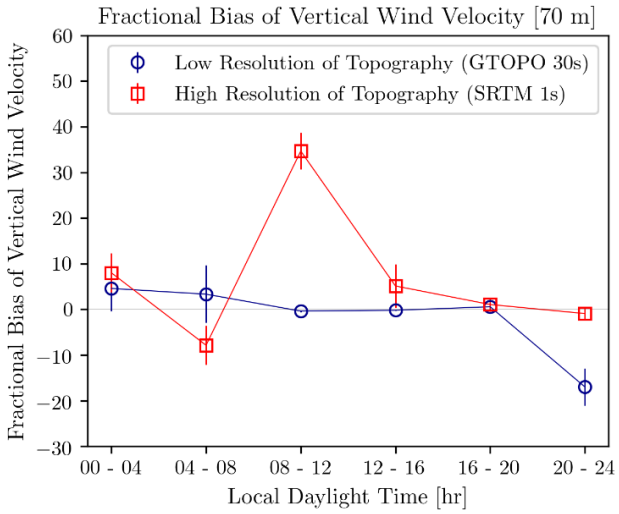

Figure 7. Fractional bias of vertical wind velocity at 70 m

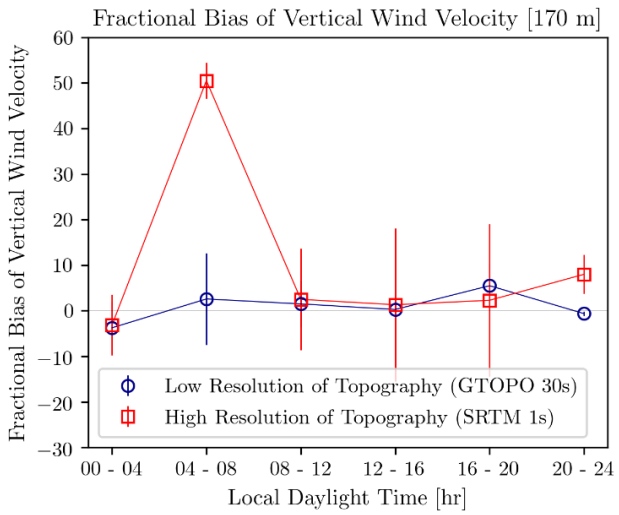

Figure 8. Fractional bias of vertical wind velocity at 170 m

The present results of vertical velocity profile show better agreements with Mini SODAR at thermally unstable condition compared to stable condition. However, there are large differences between low and high topographic resolution WRF simulations at stable conditions and with low topographic resolution WRF simulations predicting lower bias and error. Nevertheless, it should be borne in mine that, as a sonic instrument, the Mini SODAR has limitations in measuring profiles of vertical wind accurately in higher altitudes which may affect the experimental measurements.

C. Wind direction

Wind usually flows from high pressure to low pressure regions of the atmosphere. The median values of wind direction bias at 10 m (near surface level), 70 m (Mini SODAR) and 170 m (Mini SODAR) are shown in Fig. 9-11.

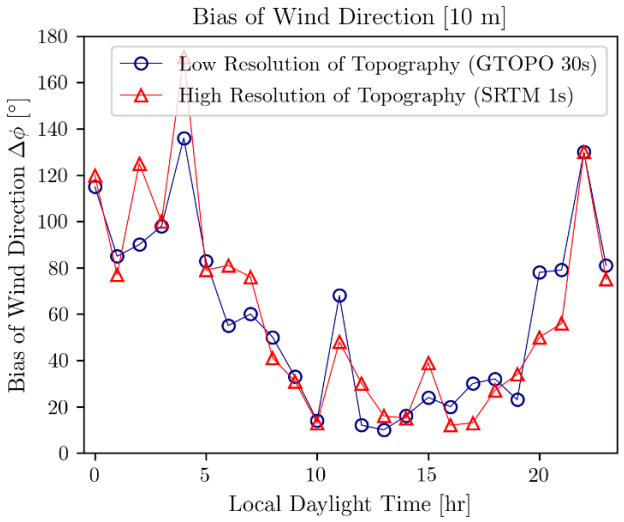

Figure 9. Median of wind direction bias at 10 m

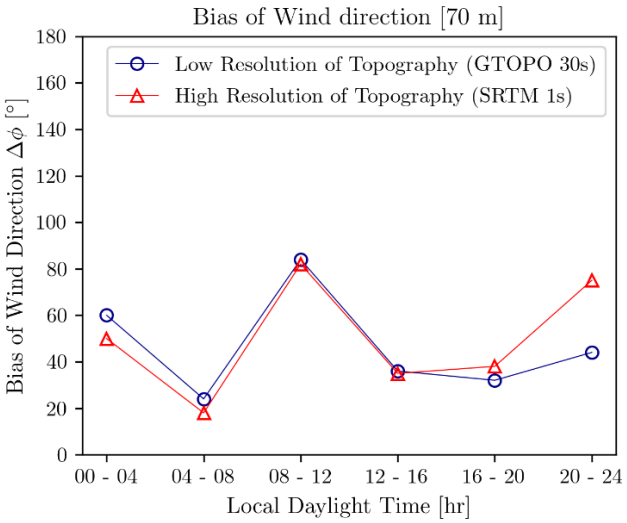

Figure 10. Median of wind direction bias at 70 m

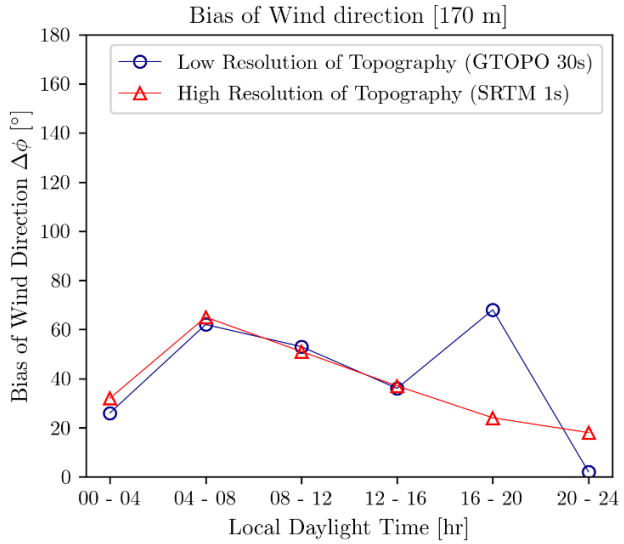

Figure 11. Median of wind direction bias at 170 m

It has been certainly identified that there is an extensive bias of wind direction in thermally stable conditions while the bias is less in unstable condition. In stable condition, the wind flows very slowly which causes more complexity to determine the exact wind direction for a specific time. Moreover, the bias of wind direction is more near surface level than the higher altitudes. This is due to the surface roughness, and shear stress which results in frequent changes of wind directions. However, there is no significant difference of wind direction between low and high topographic resolution WRF simulations during most of the times.

D. Potential temperature

Potential temperature is a more dynamically important quantity than the actual temperature as potential temperature is not affected by the physical lifting or sinking associated with flow over obstacles or large-scale atmospheric turbulence [16]. Fig. 12 shows the fractional bias of potential temperature at 2 m (near surface level) in domain 5. Figs. 13-14 show the spatial distributions of potential temperature at stable condition (0200 LDT) while Figs. 15-16 illustrate the potential temperature at unstable condition (1400 LDT) in domain 5 for low and high topographic resolutions, respectively.

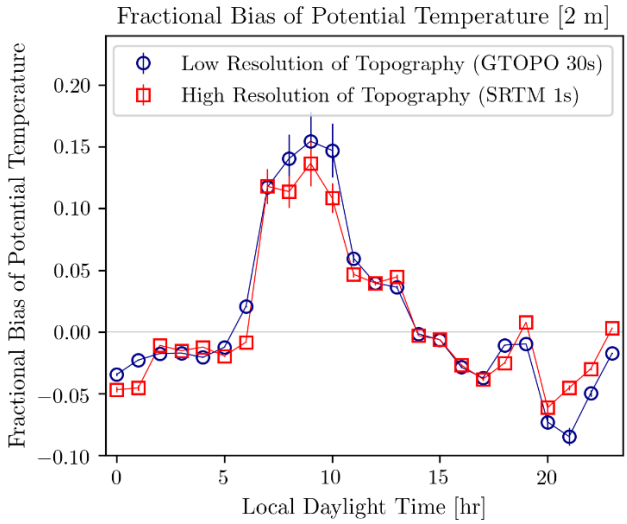

Figure 12. Fractional bias of potential temperature at 2 m

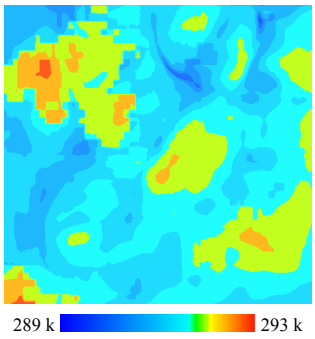

Figure 13. Potential temperature at 0200 LDT (GTOPO 30s)

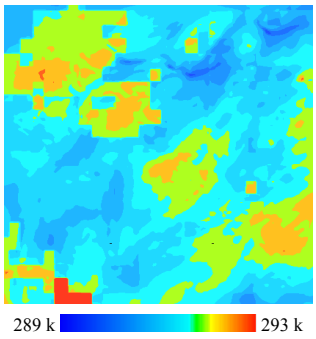

Figure 14. Potential temperature at 0200 LDT (SRTM 1s)

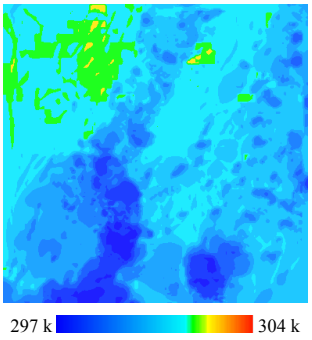

Figure 15. Potential temperature at 1400 LDT (GTOPO 30s)

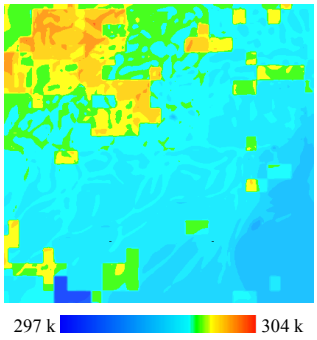

Figure 16. Potential temperature at 1400 LDT (SRTM 1s)

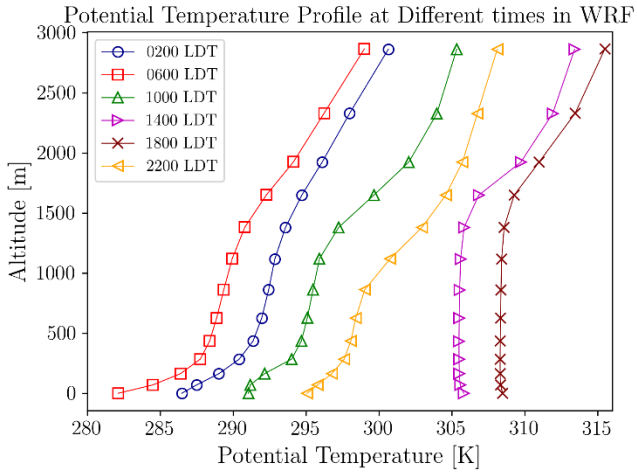

Figure 17. Potential temperature profile in WRF (SRTM)

In terms of predicting the potential temperature WRF shows better agreements at stable condition. Moreover, it has been observed that the bias is negative in stable condition which means WRF overpredicts potential temperature during this time. In contrast, WRF underestimates the potential temperature at unstable condition as the fractional bias shows positive trend during convective hours. However, the bias is almost the same in most of the times for low and high topographic resolution WRF outputs. Besides, the spatial distribution of potential temperature shows similar magnitude at stable conditions although there are much deviations of potential temperature between low and high topographic resolutions at unstable condition. It appears that the surface level temperature is better well-mixed for high topographical resolution during convective hours. This can explain the difference in the results during convective hours because surface roughness variations can possibly be responsible for a higher degree of surface level mixing. Fig. 17 shows the potential temperature profile of WRF in thermally stable and unstable conditions. When the atmosphere is stable at night and early morning, there is positive potential temperature gradient, while the potential temperature gradient is negative at lower altitudes in thermally unstable condition, especially during the afternoon hours.

E. Relative humidity

Besides water content, relative humidity depends on temperature and the pressure of the system of interest. The same amount of water vapor results in higher relative humidity in cool air than warm air. Fig. 18 shows the fractional bias of relative humidity at 2 m (near surface level) in domain 5. Moreover, the spatial distributions of relative humidity at stable condition (0200 LDT) are shown in Figs. 19-20 while the relative humidity at unstable condition (1400 LDT) in domain 5 are illustrated in Fig. 21-22 for low and high topographic resolutions.

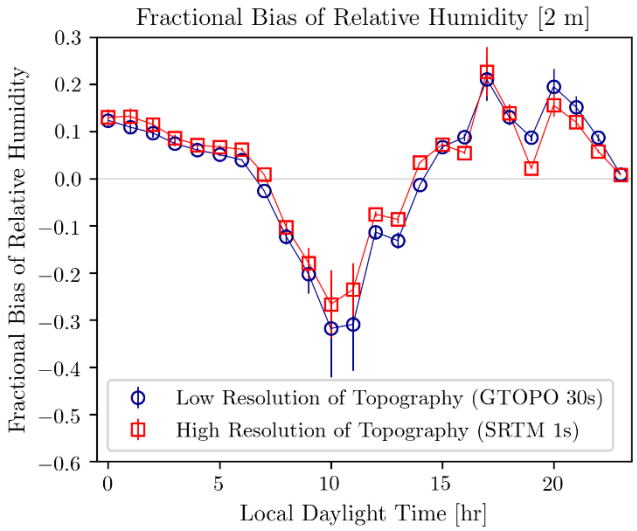

Figure 18. Fractional bias of relative humidity at 2 m

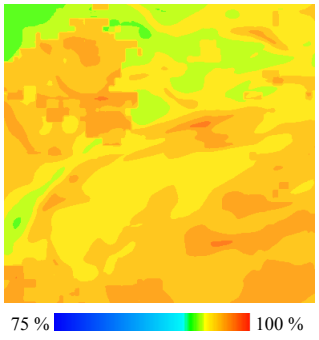

Figure 19. Relative humidity at 0200 LDT (GTOPO 30s)

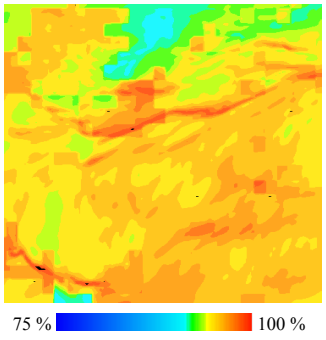

Figure 20. Relative humidity at 0200 LDT (SRTM 1s)

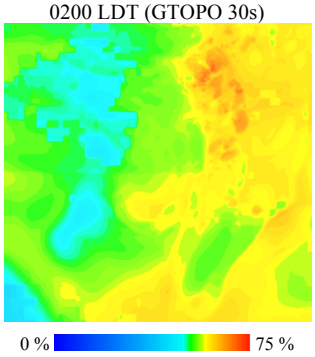

Figure 21. Relative humidity at 1400 LDT (GTOPO 30s)

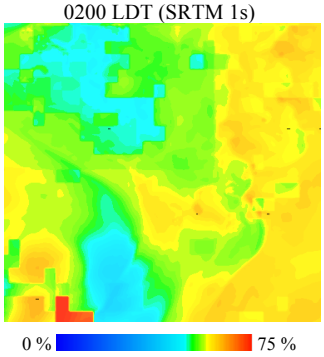

Figure 22. Relative humidity at 1400 LDT (SRTM 1s)

WRF shows a negative co-relation for fractional bias of relative humidity and temperature. WRF under predicts the relative humidity at stable condition as the bias is positive while it overestimates the relative humidity at unstable condition. However, there is no significant difference of relative humidity between low and high topographic resolution WRF outputs in both stable and unstable conditions.

F. Turbulent vertical heat flux

The turbulent vertical heat flux involves the eddy induced fluxes of heat. In vertical direction, the kinematic heat flux is denoted by $\overline{w\theta}$, where w is the standard deviation of vertical velocity and θ is the fluctuation of potential temperature [17]. At surface level, the small-scale turbulence determines the vertical heat flux while the large-scale turbulence heat flux is zero. With the increase of height, the large-scale turbulence heat flux increases and reaches to a maximum value [18].

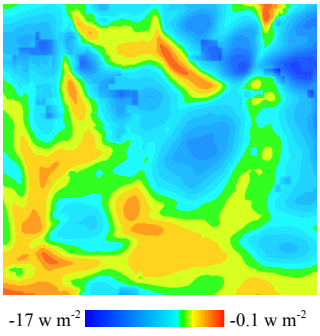

Figure 23. Vertical turbulent heat flux at 0200 LDT (GTOPO 30s)

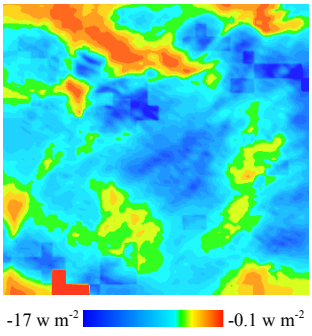

Figure 24. Vertical turbulent heat flux at 0200 LDT (SRTM 1s)

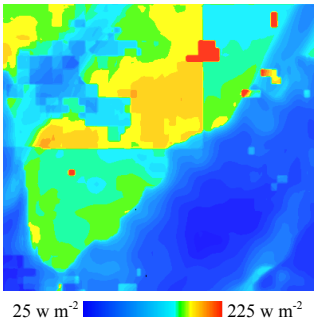

Figure 25. Vertical turbulent heat flux at 1400 LDT (GTOPO 30s)

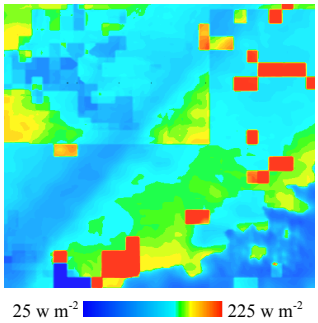

Figure 26. Vertical turbulent heat flux at 1400 LDT (SRTM 1s)

WRF shows less variations of vertical turbulent heat flux in both low and high topographic resolution simulations in stable condition. However, the differences are more at unstable condition when the heat flux changes rapidly with time. From Figs. 23-26, it has been observed that high topographic resolution WRF simulation predicts higher heat flux than the low topographic resolution WRF outputs. During convective hours, heat flux seems to exhibit a different spatial pattern between low and high topographic resolution simulations.

G. Error analysis

The results of WRF model are verified because of inherent uncertainty in model implementation at a specific location. The experimental data from the Mini SODAR and Guelph Turfgrass weather station are used to validate the WRF simulations for those specific locations in domain 5. A quantitative comparison between the experimental observations and WRF model is also performed by determining the Fractional Bias (FB) and the Normalized Mean Square Error (NMSE). Table II shows the FB and NMSE of different parameters to compare WRF outputs with experimental observations while Table III shows the optimum topographic resolutions of WRF for different properties based on the results in Table II.

TABLE II. FRACTIONAL BIAS AND NMSE OF WRF

Parameter	Fractional bias		NMSE	
	Low resolution	***High resolution***	***Low resolution***	***High resolution***
Horizontal Velocity (higher elevation)	-0.363	-0.345	0.137	0.123
Vertical Velocity (higher elevation)	0.071	0.289	0.005	0.086
Horizontal Velocity (10 m)	-0.661	-0.662	0.491	0.492
Potential temperature (2 m)	0.012	0.011	0.00014	0.00011
Relative humidity (2 m)	0.017	0.029	0.00029	0.00089

TABLE III. OPTIMUM TOPOGRAPHIC RESOLUTIONS OF WRF

Parameter	Optimum topography
Horizontal Velocity (higher elevation)	Low topographic resolution
Vertical Velocity (higher elevation)	Low topographic resolution
Horizontal Velocity (10 m)	High topographic resolution
Potential temperature (2 m)	High topographic resolution
Relative humidity (2 m)	Low topographic resolution

It is clearly identified that although there are small differences in predicting horizontal wind velocity at surface level and higher altitudes, the differences between low and high topographic resolution WRF simulations are significant in predicting the vertical wind velocity. Low topographic resolution simulations realize better results than high topographic resolution simulations as far as vertical wind is concerned. WRF over predicts the horizontal wind velocity both at surface level and higher elevation while it under predicts the vertical velocity at the measured elevations. Moreover, the bias of horizontal wind velocity is also higher at surface level compared to higher altitudes. WRF shows a correlation in fractional bias between potential temperature and relative humidity. High topographic resolution simulations produce slightly better results than low topographic resolution simulations in predicting the potential temperature while low topographic resolution simulations show better agreements with experimental observation in predicting the relative humidity.

IV. CONCLUSION

The sensitivity tests of low and high topographic resolution WRF simulations are performed to observe the urban climate both in the surface level and higher altitudes. The numerical results are compared to the experimental observations of a Mini

SODAR and Guelph Turfgrass weather station to validate the WRF outputs. Overall, the model has presented a better performance in predicting heat related properties such as temperature and relative humidity compared to the momentum related properties. It is also determined that low topographic resolution simulations show excellent agreement with observed relative humidity while high topographic resolution simulations predict the potential temperature more accurately at surface level.

On the other hand, the error of horizontal wind velocity is less with high topographic resolution WRF simulations while low topographic resolution WRF simulations deliver much better results in terms of predicting the vertical wind velocity. It is also found that predicting the surface level wind velocity is one of the main limitations of WRF as the fractional bias is almost double compared to the bias of wind velocity at higher elevations. As far as wind direction is concerned, it is also found that predictions of surface level wind direction are less reliable, specially at stable conditions, compared to wind directions at higher altitudes. However, as the atmosphere is much calm during stable hours, the wind moves very slowly which may also cause inaccurate measurement of wind directions by the anemometers and result in a large bias of wind direction in thermally stable condition.

ACKNOWLEDGMENT

The Mini SODAR was implemented with the help of Benjamin Dyer and Manoj K. Nambiar. In-kind technical support for this work was provided by Rowan Williams Davies and Irwin Inc. (RWDI). This work was supported by the Discovery Grant program (401231) from the Natural Sciences and Engineering Research Council (NSERC) of Canada; Government of Ontario through the Ontario Centres of Excellence (OCE) under the Alberta-Ontario Innovation Program (AOIP) (053450); and Emission Reduction Alberta (ERA) (053498). OCE is a member of the Ontario Network of Entrepreneurs (ONE).

REFERENCES

[1] W. C. Skamarock, J. B. Klemp, J. Dudhia, D. O. Gill, D. M. Barker, M. G. Duda, and J. G. Powers, “A description of the advanced research WRF Version 3”, NCAR technical note, Mesoscale and Microscale Meteorology Division, National Center for Atmospheric Research, Boulder, Colorado, USA, 2008.

[2] W. Y. Cheng, and W. J. Steenburgh, “Evaluation of surface sensible weather forecasts by the WRF and the Eta models over the western United States”, Weather and Forecasting, vol. 20(5), pp. 812-821, 2005.

[3] G. Roux, Y. Liu, L. D. Monache, R. S. Sheu, and T. T. Warner, “Verification of high resolution WRF-RTFDDA surface forecasts over mountains and plains”, In 10th WRF users’ workshop, pp. 20-23, 2009.

[4] J. Nossent, P. Elsen, and W. Bauwens, “Sobol’sensitivity analysis of a complex environmental model”, Environmental Modelling & Software, vol. 26(12), pp. 1515-1525, 2011.

[5] S. Hirabayashi, C. N. Kroll, and D. J. Nowak, “Component-based development and sensitivity analyses of an air pollutant dry deposition model”, Environmental Modelling & Software, vol. 26(6), pp. 804-816, 2011.

[6] R. L. Carpenter, B. L. Shaw, M. Margulis, K. S. Barr, T. Baynard, D. Yates, and J. Sharp, “Short-term numerical forecasts using WindTracer LIDAR data”, In Fourth Conference on Weather, Climate, and the New Energy Economy, American Meteorological Society, Austin, TX., 2013.

[7] D. Carvalho, A. Rocha, M. Gómez-Gesteira, and C. Santos, “A sensitivity study of the WRF model in wind simulation for an area of high wind energy”, Environmental Modelling & Software, vol. 33, pp. 23-34, 2012.

[8] N. K. Awan, H. Truhetz, and A. Gobiet, “Parameterization-induced error characteristics of MM5 and WRF operated in climate mode over the Alpine region: an ensemble-based analysis”, Journal of Climate, vol. 24(12), pp. 3107-3123, 2011.

[9] S. V. Kumar, C. D. Peters-Lidard, J. L. Eastman, and W. K. Tao, “An integrated high-resolution hydrometeorological modeling testbed using LIS and WRF”, Environmental Modelling & Software, vol. 23(2), pp. 169-181, 2008.

[10] W. Wang, C. Bruyere, M. Duda, J. Dudhia, D. Gill, H. C. Lin, and J. Mandel, “ARW version 3 modeling system user’s guide”, Mesoscale & Miscroscale Meteorology Division, National Center for Atmospheric Research, Boulder, Colorado, USA, 2015.

[11] T. G. Farr, P. A. Rosen, E. Caro, R. Crippen, R. Duren, S. Hensley, M. Kobrick, M. Paller, E. Rodriguez, L. Roth, and D. Seal, 2007, “The shuttle radar topography mission”, Reviews of geophysics, vol. 45(2), 2007.

[12] V. S. Challa, J. Indracanti, M. K. Rabarison, J. Young, C. Patrick, J. M. Baham and A. Yerramilli, “Numerical experiments on the sensitivity of WRF-CMAQ simulations of air quality in the Mississippi Gulf coastal region to PBL and Land surface models”, In The 6th Annual CMAS Conference, Chapel Hill, NC, October 13, 2007.

[13] A. A. Aliabadi, M. Moradi, D. Clement, W. D. Lubitz, and B. Gharabaghi, “Flow and temperature dynamics in an urban canyon under a comprehensive set of wind directions, wind speeds, and thermal stability conditions”, Environmental Fluid Mechanics, pp. 1-29, 2018.

[14] A. A. Aliabadi, E. S. Krayenhoff, N. Nazarian, L. W. Chew, P. R. Armstrong, A. Afshari, and L. K. Norford, “Effects of roof-edge roughness on air temperature and pollutant concentration in urban canyons”, Boundary-Layer Meteorology, vol. 164(2), pp. 249-279, 2017.

[15] D. A. Vallero, “Fundamentals of air pollution”, Academic press, 2014.

[16] J. T. Moore, "Isentropic Analysis Techniques: Basic Concepts", COMET COMAP, Retrieved on January 11, 2018.

[17] A. A. Aliabadi, “Theory and Applications of Turbulence: A Fundamental Approach for Scientists and Engineers”, Amir Abbas Aliabadi Publications, Guelph, 2018.

[18] E. Palmen, “On the mechanism of the vertical heat flux and generation of kinetic energy in the atmosphere”, Tellus, vol. 18(4), pp. 838-845, 1966